Inorganica Chimica Acta 525 (2021) 120459

Contents lists available at ScienceDirect

Inorganica Chimica Acta

journal homepage: www.elsevier.com/locate/ica

Research paper

Half-sandwich platinum group metal complexes containing coumarin-*N*-acylhydrazone hybrid ligands: Synthesis and biological evaluation studies☆

Carley Giffert L. Nongpiur [a], Lincoln Dkhar [a], Deepak Kumar Tripathi [b], Krishna Mohan Poluri [b], Werner Kaminsky [c], Mohan Rao Kollipara [a,*]

[a] Center for Advanced Studies in Chemistry, North-Eastern Hill University, Shillong 793 022, India
[b] Department of Biotechnology and Centre for Nanotechnology, Indian Institute of Technology Roorkee, Roorkee 247 667, India
[c] Department of Chemistry, University of Washington, Seattle, WA 98195, USA

ARTICLE INFO

Keywords:
Rhodium
Iridium
coumarin-*N*-acylhydrazone
Antibacterial
Antioxidant studies

ABSTRACT

A series of half-sandwich platinum group metal complexes containing coumarin-*N*-acylhydrazone ligands have been prepared. The metal precursors of the type $[(p\text{-cymene})RuCl_2]_2$ and $[Cp^*MCl_2]_2$ (M = Rh/Ir) and coumarin-*N*-acylhydrazone ligands (**L1**, **L2** and **L3**) were reacted in the ratio of 1:2 (M:L), forming neutral bidentate (N ∩ O) complexes (**1**–**9**). The complexes are of the general formula $[(arene)M\{\kappa^2_{(N\cap O)}L\}Cl]$. All these complexes have been characterized by analytical, spectroscopic and single-crystal X-ray diffraction studies. The complexes and ligands were then carried out for antibacterial, antioxidant and DNA binding studies. The results show that both ligands and complexes possess potent antibacterial and antioxidant properties.

1. Introduction

Over the years, there has been an enormous expansion in the field of organometallic chemistry due to the diverse roles that metals play in biological systems [1–4]. Several contributing factors such as high stability, high yields, less toxicity, robustness, versatility to exhibit various coordination modes and mild reaction conditions have led to an increase in the study of metals like ruthenium, rhodium and iridium [5]. In particular, arene ruthenium complexes, owing to their promising anticancer activity both in vitro and in vivo, have attracted great interest [6–9]. They have also found applications in catalysis, supramolecular assemblies and molecular devices and have shown antiviral, antibiotic and antibacterial activities [10–12]. Transition metal drug complexes are important in medical research due to their interaction with DNA. These metal complexes can target selectively particular DNA sites, which form the basis of many anticancer and antiviral drugs. Of late, several pentamethylcyclopentadienyl rhodium and iridium complexes have also been examined as prospective anticancer drugs on account of their exciting properties. Besides, they offer a high level of stability due to their relative chemical inertness [13].

The use of heterocyclic compounds as chelating ligands provides a new strategy in the design of new metallodrugs. Coumarins are an important class of naturally occurring heterocyclic compounds also known as chromen-2-one or benzopyrone. They can also be considered as lactones or cyclic esters. More than 1000 different types of coumarins have been isolated from natural sources [14]. The biological interest in coumarins derives from their versatile applications such as anticonvulsant, antidepressant, analgesic, anti-inflammatory, antimicrobial, antimalarial, antitumoral, antileukemic, antiviral, antitubercular as well as antioxidant activity [15–16]. They are also known to exhibit excellent fluorescence and DNA binding properties. Moreover, the derivatives of coumarin are considered essential for presenting anticancer properties. More specifically, 3-acetylcoumarin [17] shows a variety of biological properties and attracted intense interest as the acetyl group can be involved in Schiff base condensation with amines to give interesting biologically active compounds.

Considering the potential significance of coumarins and aromatic acid hydrazides, we are encouraged to synthesize coumarin-*N*-

☆ Dedicated to Prof. M. Palaniandavar to recognize the contributions on the occasion of his 70th birthday.

* Corresponding author.
E-mail address: mohanrao59@gmail.com (M.R. Kollipara).

https://doi.org/10.1016/j.ica.2021.120459
Received 17 February 2021; Received in revised form 21 April 2021; Accepted 14 May 2021
Available online 16 May 2021

acylhydrazone ligands, which can act as bidentate NO or tridentate ONO donor ligands upon complexation with metals. Herein, we report the synthesis of three coumarin-*N*-acylhydrazone ligands and their corresponding ruthenium, rhodium and iridium complexes. Since the ligands and complexes exhibit efficient fluorescent property, their binding property towards DNA has been studied which can prove beneficial in medicinal fields. In this present work, we have also investigated the antimicrobial and antioxidant studies for all the synthesized complexes. Ligands used in this study are presented in Chart 1.

2. Experimental section

2.1. Physical methods and materials

All the reagents required were obtained from commercial sources and used as received. Salicylaldehyde, 4-(Diethylamino) salicylaldehyde, 2-hydroxy-1-naphthaldehyde, ethyl acetoacetate, piperidine, 4-hydroxybenzhydrazide and 3-methoxybenzhydrazide were acquired from Alfa Aesar. The solvents were purified and dried before use according to the standard procedures. Ligands were prepared according to a known method (Scheme 1). Starting metal precursor complexes $[Cp^*MCl_2]_2$ (M = Rh/Ir) were prepared according to the new procedure [18] by Anton Paar Monowave 50. ^{1}H NMR spectra were recorded on a Bruker Avance II 400 MHz spectrometer using $CDCl_3$ and DMSO-d_6 as solvents; chemical shifts were referenced to TMS. Infrared spectra (KBr pellets; 400–4000 cm^{-1}) were recorded on a Perkin-Elmer 983 spectrophotometer. Mass spectra were recorded with a Waters UPLC-TQD Mass spectrometer using acetonitrile as solvent. Absorption spectra were recorded on a Perkin – Elmer Lambda 25 U.V./Visible spectrophotometer in the range of 200–800 nm at room temperature in acetonitrile.

2.2. In vitro antimicrobial assay

The antimicrobial activity of the ligands **L1**-**L3** and the newly synthesized complexes was evaluated by the agar well diffusion method. The test organisms included two Gram-positive *(Staphylococcus aureus* and *Bacillus thuringiensis*) and two Gram-negative (*Escherichia coli* and *Pseudomonas aeruginosa*) bacterial strains. The agar nutrient broth was prepared and sterilized at 121 °C for 15 min. The chosen bacterial strains were inoculated in nutrient broth and incubated overnight. Petri plates containing 30 ml of fresh Muller Hinton (M.H.) agar medium was seeded with a 24 h grown culture of bacterial strains. Wells of 5 mm diameter were cut and 100 ml of each test compound was added. Following an incubation period of the plates at 37 °C for 24 h, the antibacterial activities were evaluated by measuring the diameter of the inhibition zone formed around the well. Each experiment was performed in triplicate. For well diffusion assay 5 mg mL^{-1} of test compounds were used. DMSO was used as a negative control and the antibiotic kanamycin was applied as a positive control drug.

2.3. DPPH free radical scavenging assay

DPPH (2,2-diphenyl-1-picryl-hydrazyl) free radical scavenging assay was performed as described by Blois [19]. This method is based on the measurement of the scavenging capacity of antioxidants towards DPPH. Methanol solution of DPPH (1 ml of 0.004%) was added to 250 ml of the tested compounds dissolved in DMSO at a concentration of 1 mg/ml. The mixtures were vortexed thoroughly and kept in the dark for 30 min at room temperature. Then absorbance was measured at 517 nm using a UV–VIS spectrophotometer. For control, DMSO was added to DPPH. An ascorbic acid solution at the same concentration (1 mg/mL) was used as a standard. All the tests were performed in triplicates. The potency of scavenging the DPPH radical was calculated by measuring the percentage inhibition, *i.e.,* % DRSA = $\{(A_0 - A_1)/A_0) \times 100\}$ where A_0 is the absorbance of the control reaction, and A_1 is the absorbance of the sample considered.

2.4. Fluorescence studies on DNA interaction

DNA binding experiments of the ligand (**L2**) and complexes (**4**, **5** and **6**) were carried out using a Fluorometric assay. All experiments were done with a fixed concentration (10 μM) of the compounds under study while gradually increasing the Salmon milt (S.M.) DNA concentration (5–100 μM). For the acquisition of fluorescence emission spectrum at each concentration of DNA, the parameters used were, λ_{ex} = 429 nm;

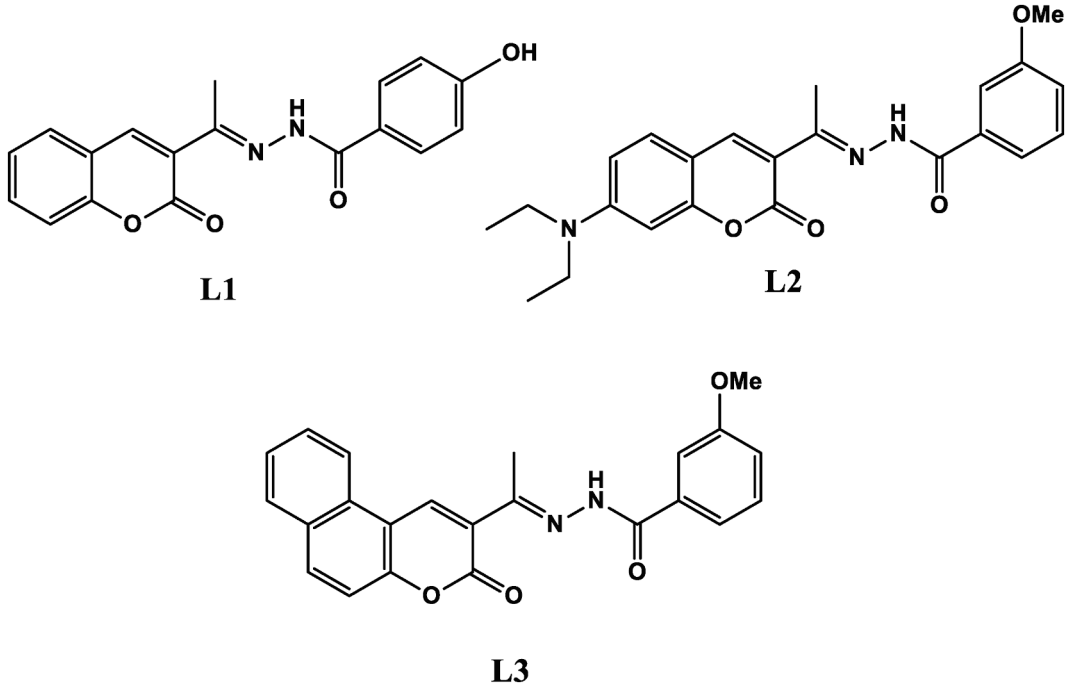

Chart 1. Ligands used in this study.

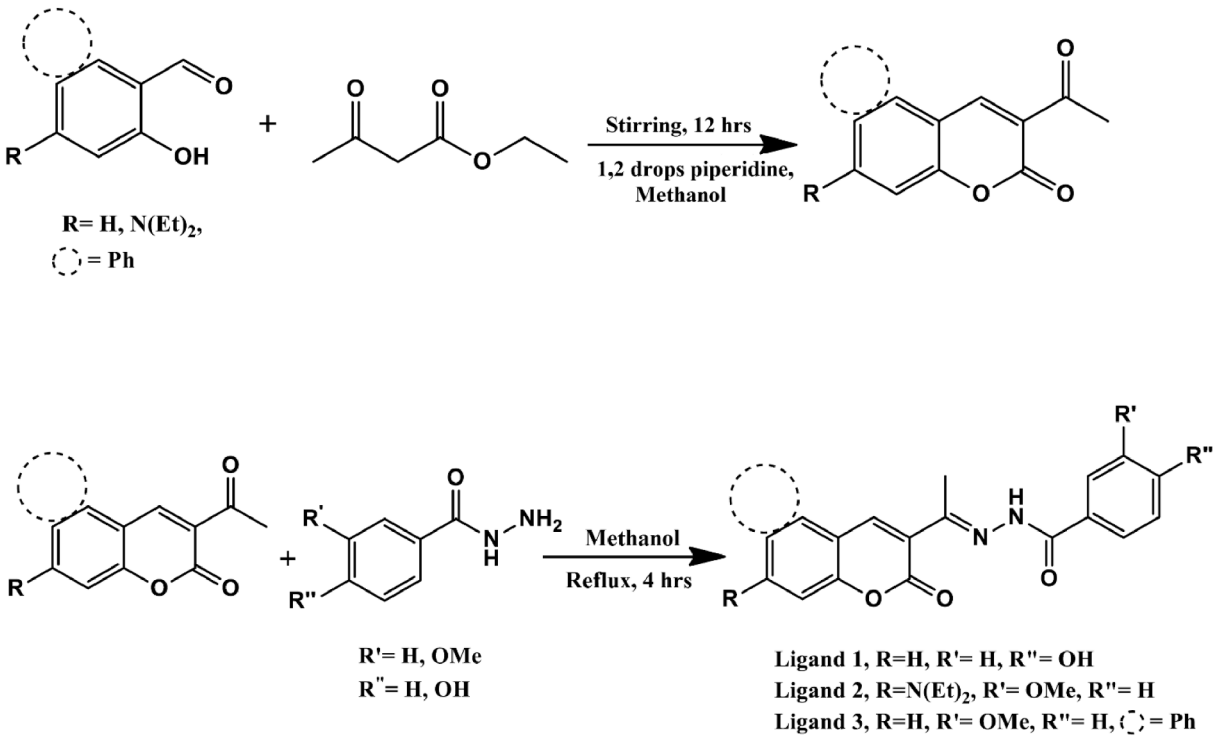

Scheme 1. Preparation of Ligands.

λ_{em} = 473 nm for ligand **L2**, and λ_{ex} = 430 nm; λ_{em} = 473 nm for complexes **4**, **5** and **6**. The dissociation constant was quantitatively analyzed using a ligand-binding model as described elsewhere [20].

2.5. General procedure for the synthesis of neutral metal complexes (1–9)

To a solution of metal precursor $[(p\text{-cymene})RuCl_2]_2$ and $[Cp^*MCl_2]_2$ (M = Rh/Ir) complexes (0.1 mmol), coumarin hydrazone ligand (**L1**, **L2 and L3**) (0.2 mmol) were added and stirred at room temperature in dry methanol (10 ml) for 4 h (Scheme 2). The product precipitated out from the reaction mixture after stirring for 1 h and stirring was continued for another 3 h to complete the reaction. The precipitate was centrifuged, washed with cold methanol (2–5 ml) and diethyl ether (2–10 ml) and air-dried.

2.5.1. *[(p-cymene)Ru($\kappa^2_{(N\cap O)}$L1)Cl]* ***(1)***

Yield : 85%; Color: Orange; IR (KBr, cm^{-1}): 3449 $\nu_{(OH)}$, 1712 $\nu_{(C=O)}$, 1608 $\nu_{(C=O)}$, 1567 $\nu_{(C=N)}$; ^{1}H NMR (400 MHz, DMSO-d_6, ppm) δ 10.58

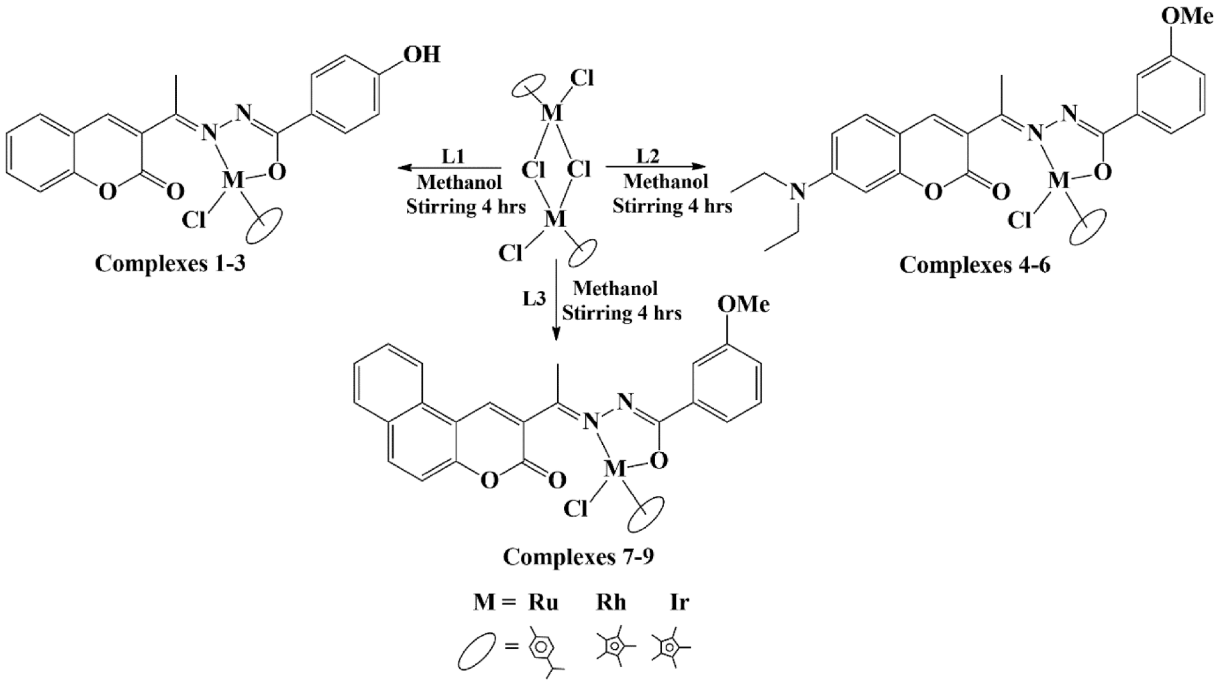

Scheme 2. Schematic representation for the syntheses of complexes.

(s, 1H), 10.02 (s, 1H), 9.86 (d, $J = 8$ Hz, 1H), 7.77 (d, $J = 8$ Hz, 1H), 7.69 (d, $J = 8$ Hz, 1H), 7.62 (d, $J = 8$ Hz, 1H), 6.87 (d, $J = 8$ Hz, 1H), 6.78 (d, $J = 12$ Hz, 1H), 6.00 (d, $J = 4$ Hz, 1H), 5.88 (d, $J = 8$ Hz, 1H), 5.81 (d, $J = 4$ Hz, 1H), 5.74 (t, $J = 8$ Hz, 2H), 5.64 (d, $J = 4$ Hz, 1H), 2.74 (sept, $J = 8$ Hz, 1H), 2.15 (s, 1H), 2.09 (s, 3H), 1.25 (d, $J = 8$ Hz, 2H), 1.21 (d, $J = 4$ Hz, 2H), 1.18 (d, $J = 8$ Hz, 2H); ^{13}C NMR (100 MHz, $CDCl_3$): δ 159.50, 155.56, 154.09, 147.74, 134.65, 131.06, 130.47, 129.71, 125.22, 118.49, 116.93, 115.01, 30.78, 22.26, 21.98, 19.17; UV–Vis {Acetonitrile, λ_{max} nm (ε,10^4 M^{-1} cm^{-1})}: 266 (2.495), 361 (1.352), 441 (1.235).

2.5.2. [Cp*Rh($\kappa^2_{(N\cap O)}$L1)Cl] (2)

Yield : 90%; Color: Orange; IR (KBr, cm^{-1}): 3445 $\nu_{(OH)}$, 1723 $\nu_{(C=O)}$, 1608 $\nu_{(C=O)}$, 1569 $\nu_{(C=N)}$; ^{1}H NMR (400 MHz, $CDCl_3$ + DMSO-d_6, ppm) δ 8.51 (s, 2H), 7.64 (m, (d, $J = 4$ Hz, 5H), 7.35 (d, $J = 12$ Hz, 2H), 7.32 (d, $J = 12$ Hz, 1H), 2.73 (s, 3H), 1.58 (s, 15H); ^{13}C NMR (100 MHz, $CDCl_3$): δ 147.73, 144.24, 134.65, 131.04, 130.66, 130.46, 128.94, 125.22, 118.48, 116.93, 116.83, 115.12, 30.78, 27.33, 9.59, 9.24, 9.09; UV–Vis {Acetonitrile, λ_{max} nm (ε,10^4 M^{-1} cm^{-1})}: 260 (3.646), 330 (2.848), 432 (1.434).

2.5.3. [Cp*Ir($\kappa^2_{(N\cap O)}$L1)Cl] (3)

Yield : 87%; Color: Yellow; IR (KBr, cm^{-1}): 3440 $\nu_{(OH)}$, 1718 $\nu_{(C=O)}$, 1608 $\nu_{(C=O)}$, 1564 $\nu_{(C=N)}$; ^{1}H NMR (400 MHz, $CDCl_3$ + DMSO-d_6, ppm) δ 10.12 (s, 1H), 9.56 (d, $J = 16$ Hz, 1H), 9.27 (d, $J = 8$ Hz, 1H), 7.83 (d, $J = 8$ Hz, 2H), 7.71 (d, $J = 8$ Hz, 1H), 7.56 (d, $J = 8$ Hz, 1H), 6.83 (m, $J = 8$ Hz, 3H), 2.59 (s, 3H), 1.74 (s, 15H); ^{13}C NMR (100 MHz, $CDCl_3$): δ 147.74, 134.65, 131.30, 130.66, 130.47, 125.23, 124.76,118.49, 116.93, 115.12, 100.21, 86.06, 85.81, 30.78, 9.30, 9.11, 8.36; UV–Vis {Acetonitrile, λ_{max} nm (ε, 10^4 M^{-1} cm^{-1})}: 275 (3.454), 312 (2.917), 445 (1.304).

2.5.4. [(p-cymene)Ru($\kappa^2_{(N\cap O)}$L2)Cl] (4)

Yield : 85%; Color: Orange; IR (KBr, cm^{-1}): 1723 $\nu_{(C=O)}$, 1663 $\nu_{(C=O)}$, 1570–1617 $\nu_{(C=N)}$; ^{1}H NMR (400 MHz, $CDCl_3$, ppm) δ 8.52 (s, 1H), 7.48 (d, $J = 8$ Hz, 2H), 7.20 (s, 1H), 6.70 (d, $J = 8$ Hz, 2H), 6.55 (s, 2H), 5.72 (d, $J = 4$ Hz, 2H), 5.64 (d, $J = 4$ Hz, 2H), 3.97 (s, 3H), 3.54 (q, $J = 8$ Hz, 4H), 3.12 (sept, $J = 8$ Hz, 1H), 2.76 (s, 6H), 2.32 (t, $J = 12$ Hz, 6H), 1.38 (d, $J = 4$ Hz, 6H); ^{13}C NMR (100 MHz, $CDCl_3$): δ 173.11, 161.03, 159.76, 158.91, 153.19, 148.03, 132.07, 129.98, 127.54, 121.10, 120.71, 116.27, 112.99, 110.03, 108.32, 102.01, 96.74, 84.30, 81.83, 79.93, 55.90, 45.30, 31.17, 30.72, 23.05, 22.35, 18.56, 12.60; UV–Vis {Acetonitrile, λ_{max} nm (ε,10^4 M^{-1} cm^{-1})}: 256 (2.652), 428 (5.726).

2.5.5. [Cp*Rh($\kappa^2_{(N\cap O)}$L2)Cl] (5)

Yield : 90%; Color: Orange; IR (KBr, cm^{-1}): 1718 $\nu_{(C=O)}$, 1660 $\nu_{(C=O)}$, 1570 $\nu_{(C=N)}$; ^{1}H NMR (400 MHz, $CDCl_3$, ppm) δ 8.43 (s, 1H), 7.48 (s, 1H), 7.44 (d, $J = 4$ Hz, 1H), 7.42 (s, 1H), 7.35 (t, $J = 8$ Hz, 1H), 7.12 (d, $J = 8$ Hz, 1H), 6.64 (d, $J = 12$ Hz, 1H), 6.47 (s, 1H), 3.85 (s, 3H), 3.45 (q, $J = 8$ Hz, 4H), 2.66 (s, 3H), 1.76 (s, 15H), 1.23 (t, $J = 8$ Hz, 6H); UV–Vis {Acetonitrile, λ_{max} nm (ε, 10^4 M^{-1} cm^{-1})}: 248 (3.292), 421 (4.546); ESI-MS (m/z): 644.59 $[M-Cl]^+$, 541.1 $[M-Rh-HCl]^+$.

2.5.6. [Cp*Ir($\kappa^2_{(N\cap O)}$L2)Cl] (6)

Yield : 82%; Color: Yellow; IR (KBr, cm^{-1}): 1723 $\nu_{(C=O)}$, 1663 $\nu_{(C=O)}$, 1565 $\nu_{(C=N)}$; ^{1}H NMR (400 MHz, $CDCl_3$, ppm) δ 8.44 (s, 1H), 7.41 (s, 1H), 7.39 (s, 1H), 7.05 (d, $J = 8$ Hz, 1H), 6.63 (d, $J = 4$ Hz, 1H), 6.60 (d, $J = 4$ Hz, 1H), 6.47 (d, $J = 4$ Hz, 2H), 3.87 (s, 3H), 3.43 (q, $J = 12$ Hz, 4H), 2.68 (s, 3H), 1.63 (s, 15H), 1.22 (t, $J = 12$ Hz, 6H); UV–Vis {Acetonitrile, λ_{max} nm (ε,10^4 M^{-1} cm^{-1})}:247 (2.641), 420 (4.476).

2.5.7. [(p-cymene)Ru($\kappa^2_{(N\cap O)}$L3)Cl] (7)

Yield : 80%; Color: Yellow; IR (KBr, cm^{-1}): 1711 $\nu_{(C=O)}$, 1634 $\nu_{(C=O)}$, 1615–1545 $\nu_{(C=N)}$, 1489–1454 $\nu_{(C=C)}$, 1138 $\nu_{(C-O)}$; ^{1}H NMR (400 MHz, $CDCl_3$ + DMSO-d_6, ppm) δ 9.82 (s, 1H), 8.71 (d, $J = 8$ Hz, 1H), 8.14 (d, $J = 8$ Hz, 1H), 7.98 (d, $J = 8$ Hz, 1H), 7.83 (t, $J = 8$ Hz, 1H), 7.76 (d, $J = 8$ Hz, 1H), 7.71 (s, 1H), 7.64 (t, $J = 8$ Hz, 1H), 7.58 (d, $J = 8$ Hz, 1H), 7.38 (s, 1H), 7.25 (t, $J = 8$ Hz, 1H), 6.95 (d, $J = 8$ Hz, 1H), 5.56 (d, $J = 4$ Hz, 1H), 5.32 (d, $J = 4$ Hz, 1H), 5.20 (d, $J = 4$ Hz, 1H), 4.09 (d, $J = 4$ Hz, 1H), 3.86 (s, 3H), 2.85 (s, 3H), 2.53 (sept, $J = 8$ Hz 1H), 1.92 (s, 3H), 1.05 (d, $J = 8$ Hz, 2H), 1.11 (d, $J = 8$ Hz, 2H); UV–Vis {Acetonitrile, λ_{max} nm (ε, 10^4 M^{-1} cm^{-1})}: 253 (3.755), 321 (2.670), 365 (2.619)); ESI-MS (m/z): 657.3 $[M+1]^+$, 621.3 $[M-Cl]^+$.

2.5.8. [Cp*Rh($\kappa^2_{(N\cap O)}$L3)Cl] (8)

Yield : 85%; Color: Orange; IR (KBr, cm^{-1}): 1721 $\nu_{(C=O)}$, 1630 $\nu_{(C=O)}$, 1590 $\nu_{(C=N)}$, 1489–1454 $\nu_{(C=C)}$, 1138 $\nu_{(C-O)}$; ^{1}H NMR (400 MHz, $CDCl_3$ + DMSO-d_6, ppm) δ 10.05 (s, 1H), 8.89 (d, $J = 8$ Hz, 1H), 8.21 (d, $J = 4$ Hz, 1H), 8.02 (d, $J = 12$ Hz, 2H), 7.81 (t, $J = 8$ Hz, 1H), 7.74 (d, $J = 4$ Hz, 1H), 7.68 (s, 1H), 7.64 (d, $J = 4$ Hz, 1H), 7.59 (d, $J = 8$ Hz, 1H), 7.29 (t, $J = 8$ Hz, 1H), 6.99 (d, $J = 8$ Hz, 1H), 3.85 (s, 3H), 2.75 (s, 3H), 1.37 (s, 15H); UV–Vis {Acetonitrile, λ_{max} nm (ε,10^4 M^{-1} cm^{-1})}: 252 (4.317), 375 (3.023); ESI-MS (m/z): 659.3 $[M+1]^+$, 623.3 $[M-Cl]^+$.

2.5.9. [Cp*Ir($\kappa^2_{(N\cap O)}$L3)Cl] (9)

Yield : 75%; Color: Yellow; IR (KBr, cm^{-1}): 1720 $\nu_{(C=O)}$, 1629 $\nu_{(C=O)}$, 1590 $\nu_{(C=N)}$, 1489–1454 $\nu_{(C=C)}$, 1138 $\nu_{(C-O)}$; ^{1}H NMR (400 MHz, $CDCl_3$ + DMSO-d_6, ppm) δ 9.91 (s, 1H), 8.69 (d, $J = 8$ Hz, 1H), 8.29 (d, $J = 12$ Hz, 1H), 8.25 (d, $J = 4$ Hz, 1H), 8.09 (d, $J = 8$ Hz, 1H), 7.82 (t, $J = 8$ Hz, 1H), 7.72 (d, $J = 8$ Hz, 1H), 7.66 (t, $J = 8$ Hz, 2H), 7.34 (t, $J = 8$ Hz, 1H), 7.05 (d, $J = 8$ Hz, 1H), 3.84 (s, 3H), 2.86 (s, 3H), 1.31 (s, 15H); UV–Vis {Acetonitrile, λ_{max} nm (ε, 10^4 M^{-1} cm^{-1})}: 214 (9.864), 304 (3.197), 366 (3.161); ESI-MS (m/z): 749.4 $[M+1]^+$, 713.4 $[M-Cl]^+$.

2.6. Structure determination by single-crystal X-ray analyses

The solvent diffusion method was used for growing single crystals. Suitable single crystals for X-ray analysis have been obtained for **1**, **7**, **8** and **9** in a dichloromethane-hexane mixture. Single crystal data for the complexes were collected with an Oxford Diffraction Xcalibur Eos Gemini diffractometer using graphite monochromated Mo-Kα radiation ($\lambda = 0.71073$ Å). The strategy for data collection was evaluated using the CrysAlisPro CCD software [21]. Crystal data were collected by standard "phi–omega scan" techniques and were scaled and reduced using CrysAlisPro RED software. The structures were solved by direct methods using SHELXS-97 and refined by full-matrix least-squares with SHELXL-97, refining on F^2 [22,23]. The positions of all atoms were obtained by direct methods. Metal atoms in the complex were located from the E-maps and all non-hydrogen atoms were refined anisotropically by full-matrix least squares. Hydrogens were placed in geometrically idealized positions and constrained to ride on their parent atoms with C—H distances of 0.95–1.00 Angstrom. Isotropic thermal parameters U_{eq} were fixed such that they were $1.2U_{eq}$ of their parent atom; U_{eq} for C.H.'s are $1.5U_{eq}$ of their parent atom U_{eq} in case of methyl groups. Crystallographic and structure refinement parameters for the complexes are summarized in Table 1 and selected bond lengths and angles are presented in Table 2. Fig. 1 was drawn with the ORTEP3 program [24].

3. Results and discussions

3.1. Synthesis of metal complexes

Treatment of d^6 halide-bridged metal dimers $[(p\text{-cymene})RuCl_2]_2$ and $[Cp^*MCl_2]_2$ (M = Rh and Ir) with the coumarin hydrazone ligands in 1:2 ratio resulted in the formation of neutral mononuclear bidentate chelated complexes **1**–**9**. Earlier reports [25] have shown that ruthenium complexes of hydrazone derivatives exhibited N∩O coordination mode as neutral complexes by deprotonation of NH proton using a base such as Et_3N. But in our case, ruthenium complexes exhibited N∩O bonding mode even without the usage of a base, as is seen in other complexes of hydrazone derivatives [26]. The same is observed for rhodium and iridium complexes. All these complexes were obtained in

Table 1
Crystal structure data and refinement parameters of complexes **1**, **7**, **8** and **9**.

Complexes	[1]	[7]	[8]	[9]
Empirical formula	$C_{28}H_{27}ClN_2O_4Ru$	C_{33} H_{31} Cl N_2 O_4 Ru	C_{33} H_{32} Cl N_2 O_4 Rh	C_{33} H_{32} Cl Ir N_2 O_4
Formula weight	592.03	656.12	658.96	748.25
Temperature (K)	293(2)	100(2)	100(2)	90(2)
Wavelength (Å)	0.71073	0.71073	0.71073	0.71073
Crystal system	triclinic	monoclinic	Orthorhombic	Orthorhombic
Space group	*P*	*C 2/c*	*P b c a*	*P b c a*
a (Å)/α (°)	10.762(2)/ 66.10(3)	23.0837(4)/ 90	12.7090(3)/ 90	12.7895(4)/ 90
b (Å)/β (°)	11.002(2)/ 80.20(3)	12.6818(3)/ 109.782(2)	21.1480(5)/ 90	21.1851(7)/ 90
c (Å)/γ (°)	12.049(2)/ 71.13(3)	20.5436(4)/ 90	21.6980(6)/ 90	21.6163(8)/ 90
Volume ($Å^3$)	1233.0(6)	5659.1(2)	5831.8(3)	5856.9(3)
Z	2	8	8	8
Density (calc) (Mg/m^{-3})	1.595	1.540	1.501	1.697
Absorption coefficient	0.783	0.691	0.718	4.691
F(0 0 0)	604.0	2688	2704	2960
Crystal size (mm^3)	0.35 × 0.19 × 0.05	0.250 × 0.200 × 0.150	0.100 × 0.070 × 0.050	0.250 × 0.200 × 0.100
Theta range for data collection	3.702 to 53.768°	2.562 to 28.273°.	2.092 to 28.286°	1.884 to 28.294°
Index ranges	$-13 \le h \le 13$, $-13 \le k \le 13$,$-15 \le l \le 15$	$-30 \le h \le 30$, $-16 \le k \le 15$,$-27 \le l \le 27$	$-16 \le h \le 16$, $-28 \le k \le 28$,$-28 \le l \le 28$	$-17 \le h \le 17$, $-28 \le k \le 28$,$-28 \le l \le 28$
Reflections collected	10,201	12,512	13,539	13,805
Independent reflections	5208 [R_{int} = 0.0598, R_{sigma} = 0.0990]	6977 [R(int) = 0.0340]	7190 [R(int) = 0.0936]	7242 [R(int) = 0.0180]
Completeness to theta = 25.00°	97.9%	99.7%	99.8%	99.7%
Absorption correction	Semi-empirical from equivalents	Semi-empirical from equivalents	Semi-empirical from equivalents	Semi-empirical from equivalents
Refinement method	Full-matrix least-squares on F^2	Full-matrix least-squares on F^2	Full-matrix least-squares on F^2	Full-matrix least-squares on F^2
Data/restraints/parameters	5208 / 0 /333	6977 / 0 / 375	7190 / 0 / 377	7242 / 0 / 377
Goodness-of-fit on F_2	0.833	0.961	0.926	1.104
Final R indices [I greater than 2sigma(I)]	R_1 = 0.0393, wR_2 = 0.0741	R1 = 0.0341, w*R2* = 0.0867	R1 = 0.0467, w*R2* = 0.0746	R1 = 0.0240, w*R2* = 0.0555
R indices (all data)Absolute structure parameter	R_1 = 0.0789, wR_2 = 0.0837n/a	R1 = 0.0494, w*R2* = 0.0950n/a	R1 = 0.1163, w*R2* = 0.0884n/a	R1 = 0.0392, w*R2* = 0.0651n/a
Largest diff. peak and hole ($e.Å^{-3}$)	0.53 and −1.17	0.911 and −0.793	0.784 and −0.959	2.370 and −0.823
CCDC No.	2,059,269	2,059,270	2,059,271	2,059,272

Structures were refined on F_0^2: w$R_2 = [\Sigma[w(F_0^2 - F_c^2)^2] / \Sigma w(F_0^2)^2]^{1/2}$, where $w^{-1} = [\Sigma(F_0^2)+(aP)^2 + bP]$ and $P = [\max(F_0^2, 0) + 2F_c^2]/3$

Table 2
Selected bond lengths (Å) and bond angles (°) of complexes.

Complexes	1	7	8	9
M(1)-CNT	1.770	1.677	1.770	1.773
M(1)-Cl(1)	2.4217(17)	2.4231(6)	2.4240(8)	2.4227(7)
M(1)-N(1)	2.098(3)			2.112(3)
M(1)-N(2)		2.1045(18)	2.133(3)	
M(1)-O(1)	2.054(3)	2.0641(15)	2.056(2)	
M(1)-O(3)				2.063(2)
N(1)- M(1)-O(1)	76.38(11)			
N(1)- M(1)-O(3)				75.62(9)
N(2)- M(1)-O(1)		75.68(6)	76.51(9)	
Cl(1)- M(1)-N(1)	86.33(10)			86.33(7)
Cl(1)- M(1)-N(2)		88.10(5)	88.62(7)	
Cl(1)- M(1)-O(1)	84.59(9)	85.32(5)	88.65(6)	
Cl(1)- M(1)-O(3)				86.53(6)

CNT represents the centroid of the *p*-cymene/Cp* ring and (M = Ru, Rh and Ir)

good yields and are yellow or orange. They are non-hygroscopic and are stable in the air as well as in a solution. These complexes show good solubility in polar organic solvents like DCM, chloroform and acetonitrile, whereas they are insoluble in non-polar solvents like hexane, diethyl ether and petroleum ether. The analytical data of these compounds are consistent with the formulations. All the coumarin hydrazone complexes were characterized spectroscopically and the molecular structures of the representative complexes were confirmed by single-crystal X-ray analysis.

3.2. Spectral studies of the complexes

3.2.1. FT-IR studies

A sharp intensity band in 1711–1726 cm^{-1} is characteristic of $\nu_{(C=O)}$ stretching of the lactone ring. It is present in the spectra of all ligands and complexes, suggests that it is not involved in coordination, also confirmed from the crystal structures. In the case of free ligands, stretching frequencies corresponding to $\nu_{(C=O)}$ of the amide group are found in 1663–1698 cm^{-1}, whereas stretching frequencies due to $\nu_{(C=N)}$ occur in the range of 1554–1635 cm^{-1}. These frequencies decrease upon complexation, which suggests coordination takes place through the azomethine nitrogen and carbonyl oxygen. The broad peak around 3428–3449 cm^{-1} can be attributed to the presence of O.H. groups in ligand **L1** and complexes **1**–**3**. In all the free ligands, stretching frequencies corresponding to the NH proton occur in the range of 3336–3463 cm^{-1} confirming that the ligands are present in the keto form. It is noteworthy that in all the synthesized complexes, a band in the range of 1608–1635 cm^{-1} characteristic of the azomethine group (-C═N-N═C-) is observed due to deprotonation and enolization of the coumarin *N*-acylhydrazone ligands and subsequent coordination through the R = N–N═C–O^- enolate form [27].

3.2.2. ^1H NMR studies of complexes

The ^1H NMR of the ligands **L1-L3** shows a singlet in the range of 9.99–10.87 ppm, which is assigned to the N.H. proton. For **L1**, the singlet corresponding to the O.H. group is observed at 10.45 ppm. The methoxy group OMe in **L2** and **L3** are observed as singlets in 3.83–3.84 ppm. The methyl protons are observed as a singlet in the range of 2.22–2.40 ppm. The signals for the diethylamino group are observed as a triplet and a quartet at 1.13 ppm and 3.44 ppm, respectively. The signals in the range of 6.57–9.30 ppm are assigned to the protons of the aromatic rings. The ^1H NMR spectra of all the complexes **1**–**9** are in good agreement with the proposed structures. The spectra of the metal complexes exhibit that the ligand resonance signals are shifted either downfield or upfield than that of the free ligands. This shift of proton signals is because of the ligand coordination to the metal atom. The absence of the N.H. peaks indicates the deprotonation of the ligands and

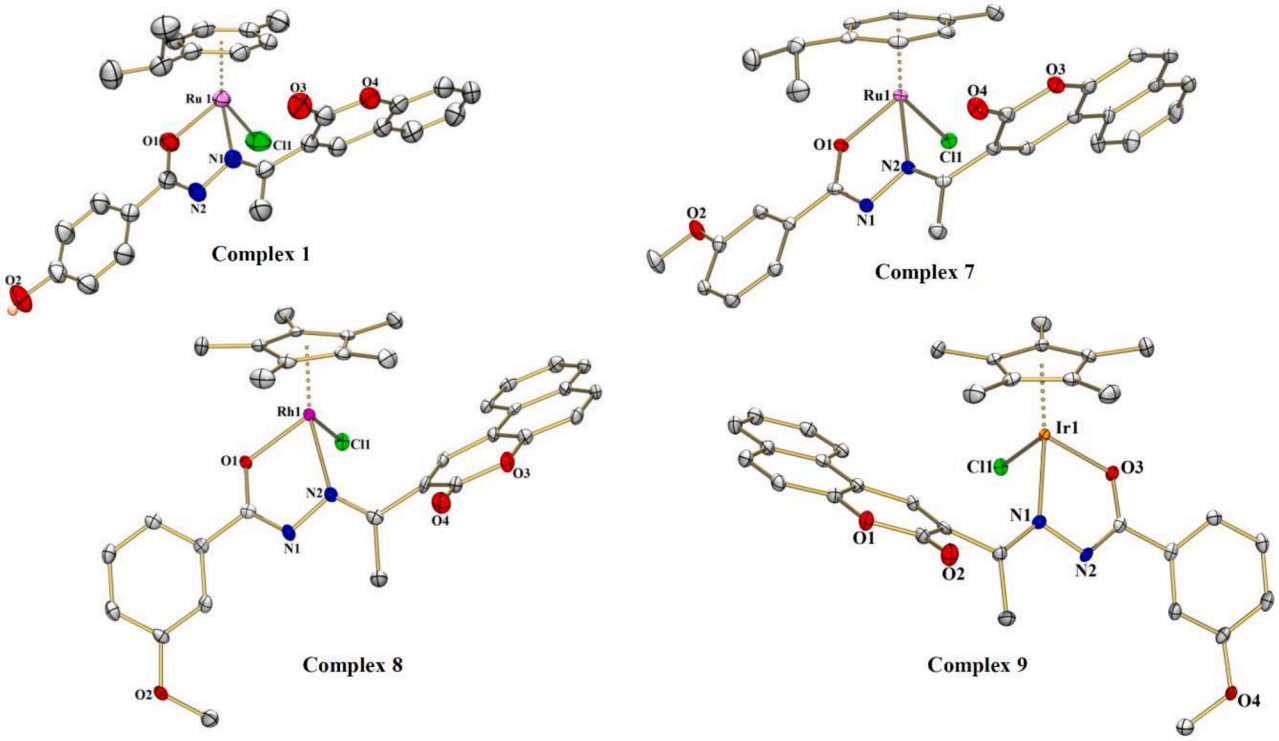

Fig. 1. ORTEP generated molecular structures of complexes **1**, **7**, **8** and **9** with 50% thermal ellipsoid probability. Hydrogen atoms (except on O2) are omitted for clarity purposes.

the existence of enolate form upon complexation. This confirmed the coordination of the ligands to the metals through the enolate-O^{-}, as is evident from the crystal structures. For complexes **1** and **3**, the signal assignable to the O.H. group is observed as singlets in the range of 10.12–10.58 ppm. For complex **2**, this signal is observed at 8.51 ppm, overlapping with the C.H. signal of coumarin moiety. The appearance of the OH signal indicates that the hydroxyl group is not involved in bonding to the metal atom. The signals for the diethylamino group are observed as triplets and quartets in the range of 1.22–2.32 ppm and 3.43–3.54 ppm, respectively. For methoxy group OMe, a sharp singlet is observed in the range of 3.84–3.97 ppm. The methyl group protons of the ligand part appeared as a singlet around 2.15–2.97 ppm. For complex **4**, this signal overlap with the methyl group protons of a *p*-cymene moiety at 2.76 ppm. Resonances due to all the aromatic protons of the ligands are observed around 5.74–10.02 ppm. In *p*-cymene complexes **1**, **4** and **7**, a sharp singlet due to the methyl group of the *p*-cymene moiety is observed in the range of 1.92–2.76 ppm. The methine proton exhibited a septet around 2.52–3.12 ppm. Usually, the two methyl groups of isopropyl substituents are observed as one doublet and the aromatic protons of the *p*-cymene ring are observed as two doublets, as seen in the spectrum of complex **4**. But in complex **1**, the methyl protons of the isopropyl group appear as three doublets around 1.18 ppm, while for complex **7**, the methyl protons of the isopropyl group appear as two doublets around 1.06 ppm. Also, the aromatic protons of the *p*-cymene ring appeared as four doublets in the range 4.10–6.01 ppm. This unusual splitting pattern is ascribed to the diastereotopic and chiral nature of the metal center or loss of symmetry of the *p*-cymene group upon coordination with the ligands [28,29]. In addition to these proton signals, a sharp singlet is observed around 1.31–1.76 ppm for the methyl protons of the Cp* ligand for the rhodium and iridium complexes. The ^{1}H NMR spectra of all the ligands and complexes are given in supplementary data (Figure S1-S12).

3.2.3. ^{13}C NMR spectra of complexes

The ^{13}C NMR spectra of the representative complexes are provided in the supplementary data (Figures S13-16). In the ^{13}C NMR spectra of the complexes, the signals in the range of 155.56–173.11 ppm are related to the ester C═O group while the signals in the range of 147.74–158.91 ppm are related to the imine C═N group. For complex **4**, the signal due to methoxy carbon is observed at 55.90 ppm. The signals due to methylene carbons and methyl carbons of the diethylamino group are observed at 45.30 and 12.60 ppm, respectively. The aromatic carbon resonances are observed in the range of 112.99–134.65 ppm. The ring carbon resonances of the *p*-cymene ligand are observed around 96.74–118.49 ppm. The methyl, methine and isopropyl carbons of *p*-cymene ligand exhibit signals in the range between 9.11 and 31.17 ppm. For complexes **2** and **3**, the signals associated with the ring carbons of the Cp* ligand are observed in the range of 85.81–94.40 ppm.

3.2.4. Mass studies of the complexes

The formation of the synthesized complexes is further supported by studying the mass spectra of some of the complexes. This study helps in establishing the structure by giving the exact molecular mass or by revealing the presence of certain structural units in a molecule. The mass spectra obtained agree well with the theoretical masses of the complexes. The mass spectra of complexes **5**, **7**–**9** are given in supplementary data (Figures S17-20). Complex **5** shows a molecular ion peak at *m/z* value 644.59, which corresponds to $[M-Cl]^{+}$ ion peak. Complexes **7**–**9** shows prominent molecular ion peaks at *m/z* values 657.3 and 621.3(**7**), 659.3 and 623.3(**8**) and 749.4 and 713.4 (**9**) identifiable to $[M + 1]^{+}$ and $[M-Cl]^{+}$ ion respectively. Also, in the case of complexes **8** and **9**, $[M-Cl]^{+}$ is most abundant, *i.e.,* the base peak showing maximum intensity in the spectra.

3.2.5. UV–Visible studies of the complexes

The electronic spectra of the ligands **L1**-**L3** and complexes **1**–**9** were recorded in acetonitrile at 10^{-4}M concentration at room temperature and scanned in the region 200–550 nm and the plot is shown in supplementary data (Figures S21-22). The electronic spectra of the ligands **L1**-**L3** display two absorption bands at 230–265 nm and 328–426 nm,

which, based on extinction coefficients, are assigned to intra-ligand π-π* and n-π* transitions respectively. The complexes displayed absorption bands at λ = 230–315 nm and 360–445 nm. Based on extinction coefficient, the higher energy absorbance band at 230–315 nm is ascribed to the intra-ligand or ligand centered transition, *i.e.,* π-π* and n-π* transitions, whereas the lower energy absorbance band at 360–445 nm is attributed to the metal to ligand charge transfer (MLCT) transition. These metal centers, low spin Ru(II), Rh(III), and Ir(III), have filled dπ (t_2g) orbitals of proper geometry which can interact or donate electrons to the empty low lying π* orbitals of the ligands [30]. For complexes **1**–**3**, the MLCT bands appear very weak due to the low concentration of the solution and are obscured by the high intense ligand bands [31]. It may also be noted that in complexes **4**–**6**, the charge transfer (C.T.) bands are shifted to longer wavelength (Red shift) and are more intense (Hyperchromic shift) compared to the other complexes with the introduction of the electron-donating auxochrome, diethylamino group as a substituent on ligand **L2**. The auxochrome provides an additional opportunity for charge delocalization and also stabilization of π* orbitals thus permitting lower energy (longer wavelength) for a transition. The stability of the complexes was examined using UV–Visible analysis by monitoring the solutions at different time intervals up to 48 h. No changes were noticed in the UV–Visible spectra signifying that all the complexes are stable at room temperature (Figures S23-24).

3.3. Description of the molecular structures of complexes

The molecular structures of the representative complexes were established by single-crystal X-ray crystallography. Atom numbering of the complexes was done by using the ORTEP program, as shown in Fig. 1. The summary of the crystal data, data collection and structure refinement parameters are summarized in Table 1. Selected bond lengths, bond angles and metal atom involving ring centroid values are listed in Table 2.

The geometry of the complexes obtained from single-crystal analyses revealed the coordination behavior of the ligands towards the metal. Single crystal analyses of the complexes also confirmed the formation of the desired product as well as the bonding modes associated with the ligand. Single crystals suitable for X-ray diffraction analysis were obtained for complexes **1**, **7, 8** and **9**. These crystals are yellow, orange and red and were obtained by the solvent diffusion method for all the complexes. In all the complexes with both ligands, the preferable mode of coordination of the metal is through the imine nitrogen and the oxygen atom with the deprotonation of the NH proton forming neutral bidentate mononuclear complexes (**1**–**9**). All these half-sandwich complexes adopt a typical three-legged "piano-stool" geometry through N ∩ O and one terminal chloride representing the three legs of a piano while the arene ring (arene = *p*-cymene, Cp*) represents the seat of a piano. Complex **1** crystallizes in the triclinic system with *P* space group, complex **7** crystallizes in monoclinic system with *C*2/*c* space group and complexes **8** and **9** crystallizes in an orthorhombic system with *Pbca* space group. The distance between the metal to the centroid of the *p*-cymene/Cp* ring of complexes **1**, **7, 8** and **9** are 1. 770 Å, 1.677 Å, 1.770 Å and 1.773 Å, respectively. The M(1)-N(1) bond distances in complexes **1** and **9** are 2.098(3) Å and 2.112(3), respectively, whereas the M(1)-N(2) bond distances in complexes **7** and **8** are 2.1047(18) Å and 2.133(3) Å respectively. The M(1)-O(1) bond distances for complexes **1**, **7** and **8** are 2.054(3) Å, 2.0641(15) Å and 2.056(2) Å respectively, while the M(1)-O(3) bond distance for complex **9** is 2.063(2) Å. The M(1)-Cl(1) bond distances for these complexes are 2.4217(17) Å, 2.4231(6) Å, 2.4240(8) Å and 2.4227(7) Å, respectively. These data are consistent with the previously reported arene metal complexes [32]. The N(1)-M(1)-O(1) bond angle value of complex **1** is 76.38(11)° and the N(1)-M(1)-O(3) bond angle value of complex **9** is 75.62(9)°. Similarly, the N(2)-M(1)-O(1) bond angles of complexes **7** and **8** are 75.68(6)° and 76.51(9)° respectively. The Cl(1)-M(1)-O(1) bond angles of these complexes are in the range of 84.59°-88.65° whereas the Cl(1)-M(1)-N(1) and Cl(1)-M(1)-N(2) bond angles are in the range of 86.33°-88.62° which are consistent with the piano stool arrangement of various groups around the metal center are comparable to previously reported values [33].

3.4. In vitro antimicrobial activity

This study is focused on exploring the antimicrobial properties of the ligands as well as the complexes. Bacterial species like *Staphylococcus aureus*, *Escherichia coli* and *Pseudomonas aeruginosa* can cause many foods borne diseases like diarrhea, vomiting, *etc*., and also healthcare-associated infections [34]. Therefore, it becomes essential to develop new metal-based antibacterial drugs that can inhibit the growth of bacteria. The antimicrobial activity of the synthesized ligands **L1**-**L3**, metal precursors and metal complexes along with the standard drug kanamycin was determined against two Gram-positive (*Staphylococcus aureus* and *Bacillus thuringiensis*) and two Gram-negative (*Escherichia coli* and *Pseudomonas aeruginosa*) bacterial strains. The results are expressed as the zone of inhibition at concentration 5 mg/ml and are given in Table 3. From the agar well diffusion study, the results unveiled that none of the compounds showed any inhibitory activity towards the Gram-negative bacterial strains (*E. coli and P. aeruginosa*) whilst some of the compounds showed positive results towards the Gram-positive bacterial strains (*S. aureus and B. thuringiensis*) (Figures S25-S26). Out of all the compounds analyzed, only complexes **3**, **4**, **5**, **6** and ligand **L3** are observed to be showing antimicrobial activity towards the Gram-positive bacterial strains, indicating selective antibacterial agents. Ligand **L3** showed activity only against *B. thuringiensis* with an inhibition value of 16 ± 1 mm. Complex **3** of **L1** showed significant activity against both *S. aureus* and *B. thuringiensis* with an inhibition value of 18 ± 1 mm, respectively. Both complex **4** and complex **6** with the same inhibition value of 19 ± 1 mm showed higher inhibitory activity towards *S. aureus* than *B. thuringiensis*. The results revealed that the coumarin hydrazone ligands showed little or no activity against all the tested organisms while some of the complexes were found to be toxic against the tested bacteria. The presence of the electron-donating groups like diethylamino and methoxy in complexes **4**, **5** and **6** might have contributed to increasing the antibacterial activity in these complexes [35]. It may be indicated that the toxicity of the metal complexes is increased compared to that of the parent ligands upon chelation. However, the activity of the complexes did not supersede the activity of the standard kanamycin. This study shows that complex **6** has the potential to be used as an antibacterial agent against Gram-positive bacteria.

The MIC value of the tested compounds ranges from 1.25 to 2.5 mg/ml against the Gram-positive bacterial strains *S. aureus and B.*

Table 3
Antibacterial activity (Agar well) of tested compounds at concentration 5 mg/mL against different bacterial strains.

Sl. No.	Compounds	Bacterial Strains Gram –ve		Gram + ve	
		E. coli	*P. aeruginosa*	*S. aureus*	*B. thuringiensis*
	Kanamycin (+ve control)	20 ± 1	22 ± 1	21 ± 1	20 ± 1
1	Ligand 1	–	–	–	–
2	Complex 1	–	–	–	–
3	Complex 2	–	–	–	–
4	Complex 3	–	–	18 ± 1	**18 ± 1**
5	Ligand 2	–	–	–	–
6	Complex 4	–	–	**19 ± 1**	16 ± 1
7	Complex 5	–	–	15 ± 1	14 ± 1
8	Complex 6	–	–	**19 ± 1**	17 ± 1
9	Ligand 3	–	–	–	16 ± 1
10	Complex 7	–	–	–	–
11	Complex 8	–	–	–	–
12	Complex 9	–	–	–	–

thuringiensis, whereas there is no inhibition observed against the Gram-negative bacterial strains by the ligands or complexes.

3.5. Antioxidative activity

Free radicals are highly reactive species that play an important role in biological processes such as metabolic pathways, cell signaling, immune response and various kinds of pathophysiological conditions. They can be both beneficial and deleterious. Aging and degenerative diseases such as heart disease, cancer, cataracts, brain dysfunction and arthritis can occur when there is oxidative damage of biomolecules such as DNA induced by excess free radicals [36]. The most effective way to eliminate free radicals that cause oxidative stress is with the help of antioxidants. Antioxidants or inhibitors of oxidation are compounds that inhibit or prevent the process of oxidation that can produce free radicals. Hence, antioxidants can act as free radical scavengers in the defense system. One of the most widely used methods to determine antioxidant activity is DPPH (2, 2-diphenyl-1-picryl-hydrazyl) free radical scavenging method. The DPPH radical scavenging assay is a decolorization assay that depends on the capacity of antioxidants to scavenge DPPH radicals. DPPH is a stable organic nitrogen-centered free radical, which is a deep purple that will decolorize when reduced into non-radical form by antioxidants. More the antioxidant activity more will be the number of DPPH radicals that will be scavenged by the antioxidants. This will make the compound an excellent antioxidant or scavenger in preventing cell damage. The percentage radical scavenging ability of the compounds was tested based on the radical scavenging effect on the DPPH free radical. Amongst the tested compounds, at a concentration of 1 mg/mL, the DPPH radical scavenging activity (DRSA%) of complexes **1**, **3**, and **6** reached more prominent than or equivalent to 50% as shown in Fig. 2 and Table 4. The iridium metal complex of **L1**, *i.e.,* complex **3** showed the highest scavenging activity at 85% while complex **1** and complex **6** showed moderate scavenging activity at 51.4% and 50.6% respectively. Other compounds also showed appreciable radical scavenging activities. The high radical scavenging activity in complex **3** may be due to the phenolic hydroxyl group, which is present as a substituent in ligand **L1**, which can provide the necessary component as a radical scavenger and hence influence the antioxidant activity. Phenolic compounds, on account of their redox properties, act as reducing agents, hydrogen donors and metal chelators and hence are considered antioxidants as they can neutralize the free radicals and inhibit the propagation of the chain reactions [37]. It may also be suggested that the chelation of the ligand with metal ions plays an important role in increasing the antioxidative properties, as is evident from the higher activities portrayed by the complexes in comparison to the parent ligands.

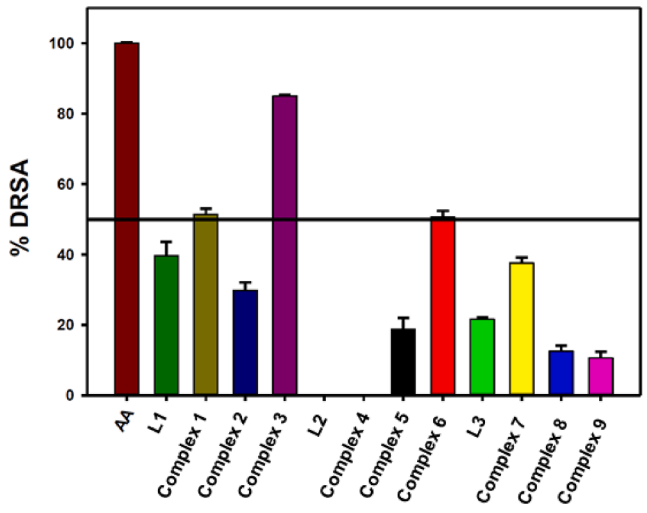

Fig. 2. Histogram of the DPPH radical scavenging activity of ligands and complexes in comparison with Ascorbic acid.

Table 4
DPPH radical scavenging activity of tested compounds.

Sl. No.	Compound	% DRSA	Std. error
1	AA	99.9	± 0.2
2	Ligand 1	39.7	± 3.9
3	Complex 1	**51.4**	± 1.6
4	Complex 2	29.9	± 2.3
5	Complex 3	**85.0**	± 0.4
6	Complex 5	18.8	± 3.2
7	Complex 6	**50.6**	± 1.7
8	Ligand 3	21.7	± 0.5
9	Complex 7	37.6	±1.6
10	Complex 8	12.5	±1.6
11	Complex 9	10.6	± 1.7

3.6. DNA binding properties

A large number of compounds can bind with the double-stranded DNA molecules through covalent and non-covalent interactions. The negatively charged phosphate backbone, the hydrogen accepting-donating sites and aromatic hydrophobic components are parts of a DNA molecule that can interact with the compounds [38]. The UV–Vis absorption spectroscopy is one of the most universally employed methods to study the binding modes and binding extent of compounds to DNA. A fixed concentration of the ligand **L2**, complexes **4**, **5** and **6** (10 μM) was titrated against increasing concentrations of Salmon milt (S.M.) DNA. To remove the absorbance of DNA itself, an equal amount of DNA was added to both the compound solution and reference solution while taking the absorption spectra. Upon addition of SM DNA to ligand **L2** and complexes **4** and **5**, no change in their fluorescence spectrum was observed, indicating that they do not bind to SM DNA (Fig. 3). On the other hand, the MLCT band of complex **6** exhibited a substantial increase in the absorbance ('hyperchromic effect') upon the addition of DNA, which reflects the significant binding tendency of the complex for DNA (Fig. 4). However, no change was observed in the position of the absorption band of the complex in the presence of DNA, suggesting the possibility of electrostatic interactions and groove (surface) binding of the metal complex. The hyperchromic effect arises mainly due to the electrostatic attraction between the charged cations which bind to DNA and the phosphate group of the DNA backbone, thereby causing a contraction and overall damage to the secondary structure of DNA [39].

To further assess the affinity of complex **6** towards double-stranded SM DNA, the intrinsic DNA dissociation constant (K_d) was determined by monitoring changes in absorbance in the MLCT band with increasing concentrations of SM DNA. The obtained dissociation constant is 37 ± 03 μM which suggests that the complex binds to DNA with moderate affinity [40]. However, the exact mode of binding to DNA cannot be concluded only by this method and more experiments are required to further clarify the binding mode.

4. Conclusion

The present study depicts the synthesis, characterization and biological evaluation of the half-sandwich complexes of coumarin-*N*-acylhydrazone ligands (**L1** − **L3**). The ligands were found to be excellent chelators for the ruthenium, rhodium and iridium metals, coordinating preferably in the enolate form (R = N − N=C − O^-) through the azomethine nitrogen and the enolate-O^-, forming a 5-membered ring around the metal by deprotonation of NH proton. All the complexes were isolated as neutral complexes. The exact structures were determined by X-ray crystallography. The results obtained from the antimicrobial activities showed that the ligands and complexes exhibit interesting selectivity in antibacterial studies, selectively inhibiting only

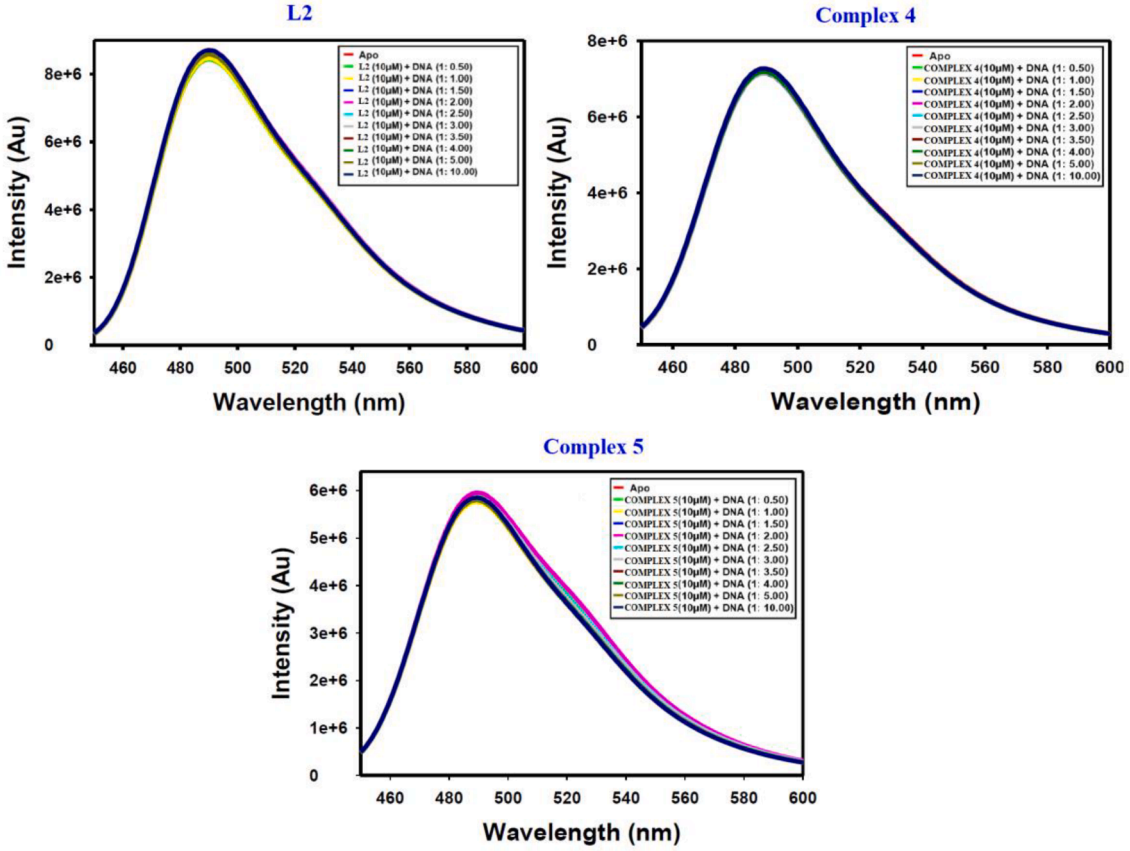

Fig. 3. The emission profile of ligand (**L2**), complex **4** and complex **5** at 10 μM in the presence of increasing concentrations of SM-DNA.

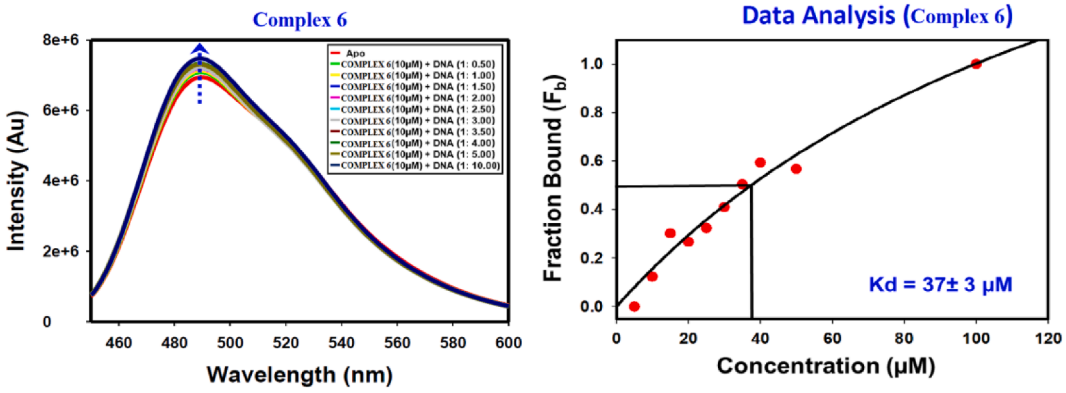

Fig. 4. The emission profile of complex **6** at 10 μM in the presence of increasing concentrations of SM-DNA. The arrow represents the changes in emission intensity upon the addition of SM-DNA.

Gram-positive bacterial strains (*S. aureus* and *B. thuringiensis*) thereby acting as selective antibacterial agents. The DPPH radical scavenging activity of the compounds revealed that complex **3** showed the highest antioxidant activity owing to the presence of the phenolic hydroxyl group attached to the ligand moiety. DNA binding studies of the fluorescent compounds with SM DNA suggest that complex **6** binds to DNA with moderate affinity *via* electrostatic interactions and groove (surface) binding. In particular, it is worth mentioning that complex **6** is observed to be a potent antimicrobial, antioxidant and DNA binding compound that can be further assessed for future use in pharmaceutical fields.

CRediT authorship contribution statement

Carley Giffert L. Nongpiur: Conceptualization, Methodology, Writing - original draft. **Lincoln Dkhar:** Formal analysis, Validation. **Deepak Kumar Tripathi:** Supervision, Visualization, Investigation. **Krishna Mohan Poluri:** . **Werner Kaminsky:** Crystal data collection, Structure solving. **Mohan Rao Kollipara:** Supervision, Visualization.

Declaration of Competing Interest

The authors declare that they have no known competing financial interests or personal relationships that could have appeared to influence the work reported in this paper.

Acknowledgment

Carley Giffert L Nongpiur thanks Professor A. K. Singh, Department of Biochemistry, NEHU, SAIF-CDRI, Lucknow and SAIF-NEHU, Shillong for spectral analyses. Carley also thank Sergei Novikov, Department of Chemistry and Chemical Biology, McMaster University, Ontario, Canada for his help with one of the crystal analyses.

Appendix A. Supplementary data

Supplementary data to this article can be found online at https://doi.org/10.1016/j.ica.2021.120459.

References:

[1] G. Gasser, I. Ott, N. Metzler-Nolte, J. Med. Chem. 54 (2011) 3.
[2] L. Ronconi, P.J. Sadler, Coord. Chem. Rev. 251 (2007) 1633.
[3] Y.K. Yan, M. Melchart, A. Habtemariam, P.J. Sadler, Chem. Commun. (2005) 4764.
[4] B. Therrien, Coord. Chem. Rev. 253 (2009) 493.
[5] A. Mandal, S. Dasgupta, S. Ganguly, A. Bauz, A. Frontera, D. Das, Dalton Trans. 46 (2017) 15257.
[6] H. Chen, J.A. Parkinson, S. Parsons, R.A. Coxall, R.O. Gould, P.J. Sadler, J. Am. Chem. Soc. 124 (2002) 3064.
[7] R.E. Morris, R.E. Aird, P.S. Murdoch, H. Chen, J. Cummings, N.D. Hughes, S. Parsons, A. Parkin, G. Boyd, D.I. Jodrell, P.J. Sadler, J. Med. Chem. 44 (2001) 3616.
[8] C.S. Allardyce, P.J. Dyson, D.J. Ellis, S.L. Heath, Chem. Commun. 1396 (2001).
[9] C. Scolaro, A. Bergamo, L. Brescacin, R. Delfino, M. Cocchietto, G. Laurenczy, T. J. Geldbach, G. Sava, P.J. Dyson, J. Med. Chem. 48 (2005) 4161.
[10] R. Lalrempuia, M.R. Kollipara, Polyhedron 23 (2003) 3155.
[11] K.S. Singh, Y.A. Mozharivskyj, M.R. Kollipara, Z. Anorg, Allg. Chem. 632 (2006) 172.
[12] K.T. Prasad, G. Gupta, A.K. Chandra, M.P. Pavan, M.R. Kollipara, J. Organomet. Chem. 695 (2010) 707.
[13] Y. Geldmacher, M. Oleszak, W.S. Sheldrick, Inorg. Chim. Acta 393 (2012) 84.
[14] A. Kotali, D.A. Nasiopoulou, C.A. Tsoleridis, P.A. Harris, C.A. Kontogiorgis, D. J. Hadjipavloulitina, Molecules 21 (2016) 138.
[15] S. Emami, S. Dadashpour, Eur. J. Med. Chem. 102 (2015) 611.
[16] H.A. Elshemy, M.A. Zaki, Bioorg. Med. Chem. 25 (2017) 1066.
[17] G. Feurer, Prog. Med. Chem. 85 (1974) 10.
[18] L. Dkhar, W. Kaminsky, K.M. Poluri, M.R. Kollipara, J. Organomet. Chem. 891 (2019) 54.
[19] M.S. Blois, Nature 181 (1958) 1199.
[20] K. Gulati, K. Gangele, D. Kumar, K.M. Poluri, Arch. Biochem. Biophys. 662 (2019) 121.
[21] Crysalis P R O, release (2012) Version 1.171.36.20. Agilent Technologies, Yarnton.
[22] G.M. Sheldrick, Acta. Cryst. A71 (2015) 3.
[23] G.M. Sheldrick, Acta. Cryst. C71 (2015) 3.
[24] L.J. Farrugia, J. Appl. Crystallogr. 30 (1997) 565.
[25] Y. Li, Z. Yang, M. Zhou, Y. Li, J. He, X. Wang, Z. Lin, RSC Adv. 7 (2017) 41527.
[26] (a) S. Aslkhademi, N. Noshiranzadeh, M.S. Sadjadi, K. Mehrani, N. Farhadyar, Polyhedron, 160 (2019) 115. (b) K. Gudasi, R. Vadavi, R. Shenoy, S. Patil, M. Nethaji, J. Coord. Chem., 60, 14 (2007) 1547. (c) R. Bikas, V. Lippolis, N. Noshiranzadeh, H. Farzaneh-Bonab, A.J. Blake, M. Siczek, H. Hosseini-Monfared, T. Lis, Eur. J. Inorg. Chem., 6 (2017) 999.
[27] I.P. Ferreira, E.D.L. Piló, A.A. Recio-Despaigne, J.G. Da Silva, J.P. Ramos, L. B. Marques, P.H.D.M. Prazeres, J.A. Takahashi, E.M. Souza-Fagundes, W. Rocha, H. Beraldo, Bioorg. Med. Chem. 24 (2016) 2988.
[28] P. Govindaswamy, B. Therrien, G. Süss-Fink, P. Štepnicka, J. Ludvík, J. Organomet. Chem. 692 (2007) 1661.
[29] R. Lalrempuia, M.R. Kollipara, P.J. Carroll, Polyhedron 22 (2003) 605.
[30] (a) T. Tsolis, M.J. Manos, S. Karkabounas, I. Zelovitis, J. Organomet. Chem., 768 (2014) 1. (b) P. Govindaswamy, J. Canivet, B. Therrien, G. Suss-Fink, P. Stepnicka, J. Ludvik, J. Organomet. Chem., 692 (2007) 3664.
[31] (a) J. Pitchaimani, M.R.C. Raja, S. Sujatha, S.K. Mahapatra, D. Moon, S.P. Anthony, V. Madhu, RSC Adv., 6 (2016) 90982. (b) M.K.M. Subarkhan, R. Ramesh, Y. Liu, New J. Chem., 40 (2016) 9813.
[32] (a) R. Payne, P. Govender, B. Therrien, C.M. Clavel, P.J. Dyson, G.S. Smith, J. Organomet. Chem., 729 (2013) 20. (b) H.S. Calik, E. Ispir, S. Karabuga, M. Aslantas, J. Organomet. Chem., 801 (2016) 122.
[33] (a) G. Gupta, S. Park, S.S. Lee, J. Kim, Z. Anorg. Allg. Chem., 637 (2011) 1516. (b) T. Tsolis, M.J. Manos, S. Karkabounas, I. Zelovitis, A. Garoufis, J. Organomet. Chem., 768 (2014) 1. (c) L. Dkhar, V. Banothu, W. Kaminsky, M.R. Kollipara, J. Organomet. Chem., 914 (2020) 121225.
[34] (a) M.B. Ferrari, S. Capacchi, G. Pelosi, G. Reffo, P. Tarasconi, R. Al-bertini, S. Pinelli, P.L. Helicin, Inorg. Chim. Acta, 286 (1999) 134. (b) L.R. Dinelli, A.A. Batista, K. Wohnrath, M.P. de Araujo, S.L. Queiroz, M.R. Bonfadini, G. Oliva, O.R. Nascimento, P.W. Cyr, K.S. MacFarlane, B.R. James, Inorg. Chem., 38 (1999) 5341.
[35] (a) A.R. Kaneria, R.R. Giri, V.G. Bhila, H.J. Prajapati, D.I. Brahmbhatt, Arab. J. Chem., 10 (2017) 1100. (b) N.C. Desai, H.M. Satodiya, K.M. Rajpara, V.V. Joshi, H. V. Vaghani, J. Saudi Chem. Soc., 21 (2017) 153.
[36] K. Tsai, T.G. Hsu, K.M. Hsu, H. Cheng, T.Y. Liu, C.F. Hsu, C.W. Kong, Free Radical Biol. Med. 31 (2001) 1465.
[37] N. Ozsoy, E. Candoken, N. Akev, Oxid. Med. Cell. Longev. 2 (2009) 99.
[38] M.M. Aleksic, V. Kapetanovic, Acta Chim. Slov. 61 (2014) 555.
[39] F. Arjmand, A. Jamsheera, Spectrochim. Acta A 78 (2011) 45.
[40] M.R. Kollipara, L. Shadap, V. Banothu, N. Agarwal, K.M. Poluri, W. Kaminsky, J. Organomet. Chem. 915 (2020), 121246.